Outage Probability Analysis and Joint Optimization for UAV-Aided FSO/RF Systems With Nonlinear Power Amplifiers

Hwi-Sung Park, Jeongju Jee, and Hyuncheol Park, *Senior Member, IEEE*

***Abstract*—The unmanned aerial vehicle (UAV)-aided free-space optical/radio frequency (FSO/RF) technique has recently attracted significant attention, which offers new possibilities thanks to its dynamic deployment capability. However, many researchers have not considered the fading characteristic of both RF and FSO links and the limited UAVs' size, weight, and power (SWAP) simultaneously. This paper focuses on a mixed FSO/RF system that facilitates the communication between a base station and mobile stations via a hovering UAV acting as a decode-and-forward relay. Considering the fading effects and the power amplifier (PA) non-linearity caused by the SWAP constraint, we mathematically analyze the closed-form and asymptotic outage probabilities. Especially in high transmit power regions, we present the destructive impact of nonlinear PAs on the outage probability and investigate modulation schemes to mitigate this degradation. The derived outage expressions match well with numerical results. Moreover, we propose a joint placement and transmit power optimization algorithm that minimizes the end-to-end outage probability with round-robin and absolute signal-to-noise ratio-based scheduling schemes. Finally, simulation results show that the performance of the proposed algorithm is comparable to that of the brute-force method.**

***Index Terms*—Unmanned aerial vehicle (UAV), free-space optics (FSO), multiple-input single-output (MISO), nonlinear power amplifier (PA), outage probability, placement, equal gain transmission (EGT).**

I. Introduction

RECENTLY, unmanned aerial vehicle (UAV) communication systems have gained significant attention as a new relay station [1], [2]. The UAV-aided systems are beneficial for combining free space optics (FSO) and radio frequency (RF) technologies. They have the capability to dynamically support large amounts of data from a base station (BS) while avoiding interference from other UAVs and multiple mobile stations (MSs) [3].

To further enhance the performance of the UAV-aided FSO/RF systems, many researchers focused on the UAV's parameter optimization algorithms and the analysis of the performance metrics [4], [5], [6], [7], [8], [9], [10], [11], [12], [13], [14], [15]. A list of existing works on UAV-aided FSO/RF systems is provided in Table I. The authors proposed the optimization algorithms considering throughput [4], latency [5], the number of MSs satisfying throughput [6], and spectral efficiency (SE) [7]. As the unlimited capacity of the FSO backhaul link was assumed in [4], [5], [6], [7], the authors in [8] presented an algorithm to jointly optimize bandwidth allocation and UAV's 3D placement by considering the capacity constraint of the FSO link. In [9], the authors optimized the trajectory of a UAV-based FSO/RF system with UAV buffer constraints and delay considerations. However, the authors in [4], [5], [6], [7], [8], [9] did not consider fading effects, which is a significant characteristic of RF and FSO channels.

On the other hand, the impact of fading on the UAV-aided FSO/RF system has been investigated in [10], [11], [12], [13], [14], [15]. In [10], the authors analyzed the outage probability, ergodic capacity (EC), and average bit-error-rate (BER) when each RF and FSO channel follows $\kappa - \mu$ fading and Málaga-$\mathcal{M}$ fading, respectively. The EC was derived in [11] for an UAV operating as both a buffer-aided and non-buffer-aided relay while accounting for the UAV's instability. By extending the system model to satellite-UAV-terrestrial networks, the authors in [12] and [13] derived various closed-form performance metrics, such as outage probability, EC, average BER, and average symbol-error-rate (SER). The authors in [14] and [15] proposed a multi-user scheduling scheme and a beamforming scheme based on the derived closed-form equation for EC, respectively. However, authors in [10], [11], [12], [13], [14], [15] did not address the practical hardware limitations of the UAV-aided relay systems.

When utilizing UAVs in mixed FSO/RF communication systems, it encounters some crucial challenges. Due to UAVs' limited size, weight, and power (SWAP), UAVs cannot adopt complex, power-intensive, and linear hardware components [1]. This constraint can result in hardware limitations on the UAV. As Table I reveals, the existing works on UAV-aided FSO/RF systems do not focus on the practical limitations and unique characteristics of UAVs. A crucial challenge that needs to be

Manuscript received 28 July 2023; revised 15 September 2023; accepted 27 September 2023. Date of publication 2 October 2023; date of current version 6 November 2023. This work was supported by the Ministry of Science and ICT (MSIT), Korea, supervised by the Institute for Information and Communications Technology Planning and Evaluation (IITP) through Information Technology Research Center support Program (ITRC) under Grant IITP-2023-RS-2023-00259991. *(Corresponding author: Hyuncheol Park.)*

Hwi-Sung Park is with the School of Electrical Engineering, Korea Advanced Institute of Science and Technology, Daejeon 34141, South Korea, and also with the Agency for Defense Development, Daejeon 34186, South Korea (e-mail: winzip90@kaist.ac.kr).

Jeongju Jee and Hyuncheol Park are with the School of Electrical Engineering, Korea Advanced Institute of Science and Technology, Daejeon 34141, South Korea (e-mail: ji1718@kaist.ac.kr; hcpark@kaist.ac.kr).

Digital Object Identifier 10.1109/JPHOT.2023.3321144

TABLE I
COMPARISON OF THE PROPOSED WORK WITH OTHER EXISTING STUDIES

Ref.	Channel fading	UAV's hardware limitations	Performance analysis metrics	Optimization parameters
[4]	✗	Limited transmit power	Throughput	Bandwidth allocation, Transmit power 3D Placement
[5]	✗	✗	Latency	Bandwidth allocation, User association, 3D Placement
[6]	✗	✗	The No. of MSs	Bandwidth allocation, User association, 3D Placement
[7]	✗	✗	SE	User association, 3D Placement
[8]	✗	✗	The No. of MSs	Bandwidth allocation, 3D Placement
[9]	✗	✗	Throughput	Trajectory
[10]	$\mathcal{O}$	✗	Outage probability, EC, BER	✗
[11]	$\mathcal{O}$	✗	EC	✗
[12]	$\mathcal{O}$	✗	Outage probability, EC, BER	✗
[13]	$\mathcal{O}$	✗	Outage probability, EC, SER	✗
[14]	$\mathcal{O}$	✗	EC	Multiuser scheduling
[15]	$\mathcal{O}$	✗	EC	Beamforming
Proposed work	$\mathcal{O}$	Nonlinear PAs, Limited battery Limited transmit power	Outage probability	Transmit power, 3D Placement

addressed is the non-linearity of power amplifiers (PAs), which can degrade the overall performance of UAV-aided relay systems [16]. Moreover, UAVs are equipped with onboard batteries that have limited capacity, which can restrict their travel distance and transmit power to support MSs [17], [18], [19]. Lastly, both RF and FSO systems consider outage probability as a crucial factor in determining the optimal location for UAV [20], [21]. Therefore, optimizing the joint UAV placement and transmit power based on outage probability is essential for practical UAV-aided FSO/RF systems, considering fading effects, nonlinear PAs, and limited battery.

In this paper, we focus on a mixed FSO/RF system that employs a single UAV-aided decode-and-forward (DF) relay with nonlinear PAs. The UAV relay serves multiple MSs with conventional scheduling schemes such as round-robin (RR) or absolute signal-to-noise ratio-based (ASB) scheduling. The FSO link model considers channel factors such as atmospheric loss, turbulence, angle of arrival (AoA) fluctuation, and pointing error loss [22], [23]. For the RF link of our system model, we consider multiple-input single-output (MISO) under nonlinear PAs and equal gain transmission (EGT) beamforming. Furthermore, the RF links are modeled as frequency flat Nakagami-m fading channels, which is a practical assumption for the hovering UAV-to-ground communication scenario in a line-of-sight environment [11], [24]. The contributions of this paper are summarized as follows:

- Considering nonlinear PAs and fading effects in UAV-aided FSO/RF systems, we mathematically derive the closed-form expressions of the end-to-end outage probability. We confirm that our mathematical analysis matches with numerical results. Moreover, our results reveal that optimizing transmit power and 3D placement is necessary to enhance the outage probability of the UAV-aided FSO/RF system.
- We derive an asymptotic outage probability to observe the effect of nonlinear PAs with per-antenna transmit power. In the high-transmit power region, the end-to-end outage probability approaches one due to the presence of signal-to-noise-and-distortion ratio (SNDR) ceilings. This observation reveals that the nonlinear characteristics of the PAs fundamentally limit the system's performance.
- Our paper indicates that the modulation schemes significantly affect the performance of the systems with nonlinear PAs. We derive that the outage probability and the SNDR ceilings are quantified explicitly using the moments of modulated symbols. By implementing suitable modulation schemes, we can effectively mitigate the effect of nonlinear PAs.
- In terms of minimizing the derived outage probability, we finally propose an algorithm for optimizing the UAV's transmit power and 3D placement concerning the battery and transmit power limitations. Specifically, we divide the optimization problem into two subproblems and propose an iterative algorithm to solve the transmit power and the 3D placement alternately. The proposed algorithm can adopt conventional RR and ASB scheduling schemes. Numerical

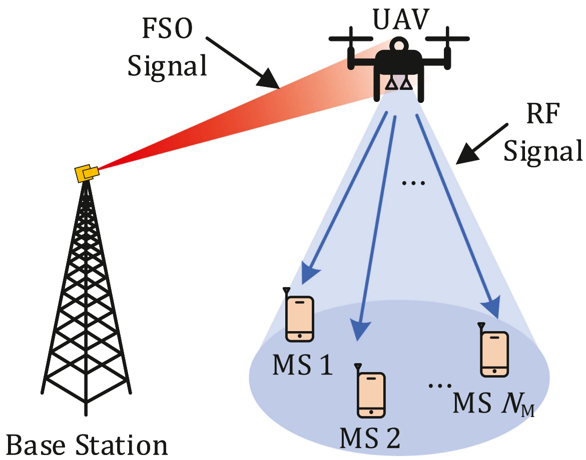

Fig. 1. UAV-aided FSO/RF relaying system with N_{M} MSs.

results verify that our proposed algorithm performs comparably to the Brute-force Search, which is the optimal baseline scheme.

The rest of the paper is organized as follows. First, Section II presents the system model for UAV-aided FSO/RF systems. In Section III, we analyze closed-form and asymptotic outage probability. Section IV formulates the outage probability minimization problem and proposes an algorithm that optimizes the UAV's transmit power and 3D placement. In Section V, we offer numerical simulation results on the proposed algorithm. Finally, our conclusions are summarized in Section VI.

Notations: Bold lowercase letters denote vectors, $(\cdot)^{\mathrm{T}}$ and $(\cdot)^*$ indicate the transpose and conjugate operation, respectively. $\mathrm{diag}(\mathbf{x})$ denotes the diagonal matrix with the elements of $\mathbf{x}$; $|\cdot|$ and $||\cdot||$ denote the absolute value and Euclidean norm, respectively; $\mathbb{E}[\cdot]$ represents the expectation; $\mathbb{C}^{M\times N}$ denotes the complex space of $M \times N$; $\mathcal{CN}(\mu, \sigma^2)$ represents the complex Gaussian distributions with mean μ and covariance σ^2; $Nakagami(m, \omega)$ denotes the Nakagami-m distribution with severity parameter m and average power ω; and $\mathrm{Re}(x)$ represents the real part of x.

II. System Model

In this section, we provide a system model of a UAV-aided DF relaying system in a mixed FSO/RF environment as illustrated in Fig. 1. The BS transmits an optical signal to the UAV via an FSO link. The UAV, acting as the DF relay node, receives the optical signal and converts it into electrical signals. Then, the UAV transmits RF signals to N_{M} MSs via N_{T} antennas with nonlinear PAs. The MSs, having a single antenna each due to size limitations, are served by the UAV using either the RR or the ASB scheduling scheme. Note that our system model has no direct communication link between the BS and the MSs due to severe blockage and the directionality of the FSO link.

A. FSO Link

First, the BS transmits the optical signal x_f to the UAV through the FSO link. The received FSO signal at the UAV can be expressed as

$$y_f = I_f x_f + n_f, \tag{1}$$

where x_f is the transmit optical signal with a total power constraint of $\mathbb{E}[|x_f|^2] \le P_f$ and n_f is an additive white Gaussian noise (AWGN) with $n_f \sim \mathcal{CN}(0, \sigma_f^2)$. The noise variance on the FSO link is given as $\sigma_f^2 = N_f B_f$ where N_f is the noise power spectral density and B_f is the FSO bandwidth. The FSO channel gain I_f in (1) can be expressed as

$$I_f = I_p I_a I_{pg} I_{pa}, \tag{2}$$

where $I_p = \exp(-D_f \xi)$ is an atmospheric loss with scattering coefficient ξ and FSO link distance $D_f = ||\mathbf{r}_u - \mathbf{r}_s||$. Here, $\mathbf{r}_s = (x_s, y_s, z_s)$ and $\mathbf{r}_u = (x_u, y_u, z_u)$ are the 3D position of BS and UAV, respectively [22], [23]. Moreover, I_a represents atmospheric turbulence, I_{pg} is the pointing error loss due to the deviation between the receiver lens center and the received beam center, and I_{pa} is a link interruption due to AoA fluctuations. The turbulence-induced fading I_a is modeled as Gamma-Gamma distribution with the effective numbers of large-scale and small-scale turbulence cells given as

$$\alpha_f = \left[\exp\left(\frac{0.49\sigma_R^2}{\left(1+1.11\sigma_R^{\frac{12}{5}}\right)^{\frac{7}{6}}}\right)-1\right]^{-1}, \tag{3}$$

and

$$\beta_f = \left[\exp\left(\frac{0.51\sigma_R^2}{\left(1+0.69\sigma_R^{\frac{12}{5}}\right)^{\frac{5}{6}}}\right)-1\right]^{-1}, \tag{4}$$

respectively [25]. The Rytov variance is defined as $\sigma_R^2 = 1.23 C_n^2 k_f^{7/6} D_f^{11/6}$ where k_f is the wave number defined as $k_f = 2\pi/\lambda_f$ with the wavelength for the FSO link λ_f. The refractive-index structure parameter C_n^2 depends on atmospheric altitude and is evaluated from the Hufnagel-Valley (H-V) model described by $C_n^2 \approx C_n^2(0)\exp(\frac{-z_u}{100})$, where $C_n^2(0)$ denotes the nominal value at the ground [11], [26].

B. RF Links With Nonlinear PAs

Next, the DF-based UAV relay decodes the received signal y_f and re-encodes it to s, which is a complex data symbol with arbitrary modulation satisfying $\mathbb{E}[ss^*] = 1$. Before amplification by the nonlinear PAs, the RF transmit signal for the kth MS can be expressed as

$$\mathbf{u}_k = \sqrt{P_r}\mathbf{w}_k s, \tag{5}$$

where P_r is the transmit power of RF links. The EGT beamforming vector denotes $\mathbf{w}_k = [w_{1,k}, \ldots, w_{N_{\mathrm{T}},k}]^{\mathrm{T}}$ satisfying $||\mathbf{w}_k||^2 = 1$, where $w_{n,k} = \frac{1}{\sqrt{N_{\mathrm{T}}}}\exp(-\iota\angle h_{n,k})$ with $\angle h_{n,k}$ denoting the phase of $h_{n,k}$ and $\iota = \sqrt{-1}$. After passing through the nonlinear PAs, the signal $\mathbf{x}_k$ can be expressed as

$$\mathbf{x}_k = \sum_{p=1}^{Q} \alpha_p \mathrm{diag}\left(|\mathbf{u}_k|^{p-1}\right)\mathbf{u}_k, \tag{6}$$

where α_p denotes the pth-order coefficient for the input-output characteristic of the PA, and Q is the number of nonlinear components [16], [27]. Finally, the received signal at the kth MS is described as

$$y_k = g_k \mathbf{h}_k^{\mathrm{T}} \mathbf{x}_k + n_r, \tag{7}$$

where g_k represents the free-space path loss which is typically modeled as $g_k = \frac{1}{c_r D_k}$. Here, $c_r = \frac{f}{23.85}$ with the center frequency f in MHz and D_k denote the RF link distance satisfying $D_k = ||\mathbf{r}_k - \mathbf{r}_u||$ with the position of the kth MS $\mathbf{r}_k = (x_k, y_k, z_k)$ [11]. The RF fading coefficient $\mathbf{h}_k$ in (7) denotes as $\mathbf{h}_k = [h_{1,k}, \ldots, h_{N_{\mathrm{T}},k}]^{\mathrm{T}}$ where $h_{n,k}$ is the complex channel gain satisfying $|h_{n,k}| \sim Nakagami(m_k, \omega)$. We consider a relationship between m_k and $\theta_k \in [0, \pi/2]$ characterized by $m_k = m_{\min} \exp(m_p \theta_k)$ where $m_p = \frac{2}{\pi} \ln\left(\frac{m_{\max}}{m_{\min}}\right)$, $m_{\min}$ and $m_{\max}$ are the minimum and maximum values of m_k, respectively. Also, θ_k denotes the elevation angle defining $\theta_k = \arcsin\left(\frac{|z_u - z_k|}{D_k}\right)$. Note that when the multipath fading gets its highest level (i.e., $\theta_k = 0$), m_k reaches $m_{\min}$, whereas for $\theta_k = \pi/2$, m_k has approaches $m_{\max}$. In addition, n_r in (7) is an AWGN with $n_r \sim \mathcal{CN}(0, \sigma_r^2)$. The noise variance in the RF channel is given as $\sigma_r^2 = B_r N_r N_0$ where B_r is the RF bandwidth, N_r is the receiver noise figure, and N_0 is the noise power spectral density.

III. Outage Probability

This section presents the outage probability analysis for the mixed FSO/RF UAV-aided systems. Based on the received signals of individual links, we derive the end-to-end and asymptotic outage probabilities. To validate our analysis, we simulate the outage probability and compare the results with our numerical calculations.

A. FSO Link

By assuming intensity modulation/direct detection (IM/DD) modulation, the signal-to-noise-ratio (SNR) at UAV can be expressed from (1) as

$$\gamma_f = \frac{P_f^2 |I_f|^2}{\sigma_f^2} = \frac{\bar{\gamma}_f |I_f|^2}{(I_p A_0)^2}, \tag{8}$$

where $\bar{\gamma}_f = \frac{(P_f I_p A_0)^2}{\sigma_f^2}$ and A_0 is the fraction of the collected power at the center of the receiver lens. Then, the cumulative distribution function (CDF) of γ_f is given as [23]

$$F_{\gamma_f}(\gamma) \simeq a_1 + (1 - a_1) \sum_{n=0}^{N_c} \left(\frac{c_1}{\tau} \left(\frac{\gamma}{\bar{\gamma}_f} \right)^{\frac{\tau}{2}} + \frac{c_2}{n + \alpha_f} \left(\frac{\gamma}{\bar{\gamma}_f} \right)^{\frac{n+\alpha_f}{2}} - \frac{c_3}{n + \beta_f} \left(\frac{\gamma}{\bar{\gamma}_f} \right)^{\frac{n+\beta_f}{2}} \right), \tag{9}$$

where $a_1 = \exp(-\frac{\theta_{\mathrm{FOV}}^2}{2(\sigma_{so}^2 + \sigma_{ro}^2)})$ with field-of-view (FoV) angle θ_{FOV}, the standard deviations for orientation of the transmit node σ_{so}^2 and the receiver node σ_{ro}^2. Additionally, N_c is the coefficient depending on the Rytov variance σ_R^2 and τ is the ratio between the equivalent beam radius and the pointing error displacement standard deviation at the receiver given as $\tau = \frac{w_{zeq}^2}{4(\sigma_{sp}^2 + \sigma_{rp}^2)}$, where w_{zeq}^2 is the equivalent beam waist, σ_{sp} and σ_{rp} are the standard deviations for the position of the transmit and the receiver node, respectively. The coefficients c_1, c_2 and c_3 in (9) are represented in Appendix A.

B. RF Links With Nonlinear PAs

By using the Bussgang theorem [28], we can decompose $g_k \mathbf{h}_k^{\mathrm{T}} \mathbf{x}_k$ in (7) into the component linearly correlated with s and the rest uncorrelated terms as

$$y_k = G_k s + d_k + n_r, \tag{10}$$

where G_k is the linearity coefficient following $G_k = \frac{\mathbb{E}[y_k s^*]}{\mathbb{E}[ss^*]}$ and d_k denotes the residual distortion uncorrelated with s. Considering the nonlinear PAs and EGT beamforming, the SNDR of the RF links is as follows [16]

$$\gamma_k = \frac{|G_k|^2}{\sigma_k^2 + \sigma_r^2} = \frac{g_k^2 H_k^2 K}{g_k^2 H_k^2 L + \sigma_r^2}, \tag{11}$$

where σ_k^2 is the variance of d_k, $H_k = \sum_{n=1}^{N_{\mathrm{T}}} |h_{n,k}|$, $K = \sum_{i=1}^{Q} \sum_{j=1}^{Q} \alpha_i \alpha_j^* S_{i,j}^S P_a^{\frac{i+j}{2}}$, and $L = \sum_{i=1}^{Q} \sum_{j=1}^{Q} \alpha_i \alpha_j^* S_{i,j}^D P_a^{\frac{i+j}{2}}$ with per-antenna transmit power $P_a = \frac{P_r}{N_{\mathrm{T}}}$, $S_{i,j}^S = S_{i+1} S_{j+1}$, $S_{i,j}^D = S_{i+j} - S_{i+1} S_{j+1}$, and $S_i = \mathbb{E}[|s|^i]$. Note that K and L result in a non-monotonic relationship between γ_k and P_a. Specifically, the uncorrelated distortion L is smaller than the desired signal K in the low-power regions. However, L increases faster than K, which reduces the SNDR in the high-power regions [29], [30]. Moreover, for the system with nonlinear PAs, γ_k is a function of the modulation schemes since S_i is determined by the constellation points of modulation schemes. On the other hand, for the system with linear PAs, i.e., $\alpha_1 = 1$, $\alpha_i = 0 \; \forall i \geq 2$, we can obtain $K = P_a$ and $L = 0$ with $S_2 = 1$, implying that γ_k and modulation schemes are unrelated. In the following proposition, we derive the CDF of SNDR γ_k based on (11).

Proposition 1: The CDF of γ_k under the nonlinear PAs, EGT beamforming and independent and identically distributed (i.i.d.) Nakagami-m fading channels can be approximated as

$$F_{\gamma_k}(\gamma) \approx \begin{cases} 1 - \frac{1}{\Gamma(M_k)} \Gamma\left(M_k, \frac{M_k \gamma \sigma_r^2}{\Omega_k g_k^2 (K - \gamma L)}\right), & \gamma < \frac{K}{L}, \\ 1, & \gamma \geq \frac{K}{L}, \end{cases} \tag{12}$$

where $M_k = m_k N_{\mathrm{T}}$, $\Omega_k = \omega N_{\mathrm{T}} (1 + \frac{(N_{\mathrm{T}} - 1) \Gamma^2(m_k + \frac{1}{2})}{m_k \Gamma^2(m_k)})$, $\Gamma(\cdot)$ and $\Gamma(\cdot, \cdot)$ are the gamma function and the upper incomplete gamma function, respectively.

Proof: The CDF of γ_k can be expressed as

$$F_{\gamma_k}(\gamma) = \Pr(\gamma_k \leq \gamma) = \Pr\left(H_k^2 \leq \frac{\sigma^2 \gamma}{g_k^2 (K - \gamma L)} \right). \tag{13}$$

If $K - \gamma L \leq 0$, then the inequality is satisfied for any realization of the non-negative variable H_k^2 [31]. Since the sum of i.i.d. Nakagami-m random variables H_k can be approximated accurately by $H_k \sim Nakagami(M_k, \Omega_k)$ [32], the CDF of H_k^2 can be expressed as

$$F_{H_k^2}(x) \approx 1 - \frac{1}{\Gamma(M_k)}\Gamma\left(M_k, \frac{M_k x}{\Omega_k}\right). \tag{14}$$

Substituting (14) into (13), we can obtain (12). □

In the special case of the single-input single-output (SISO) system with the ideal PA, i.e., $\alpha_1 = 1$, $\alpha_i = 0\ \forall i \geq 2$, and $N_{\mathrm{T}} = 1$, we can reduce (12) to the conventional result of [32], $F_{\gamma_k}^{id}(\gamma) = 1 - \frac{1}{\Gamma(m_k)}\Gamma(m_k, \frac{m_k\gamma}{\bar{\gamma}_{r,s}^{\mathrm{id}}})$ where $\bar{\gamma}_{r,s}^{\mathrm{id}} = \frac{g_k^2 \omega P_r}{\sigma_r^2}$. The UAV serves multiple MSs by employing multi-user scheduling schemes, and the resulting CDF can be expressed as follows. For the RR scheduling, each MS has an equal chance to receive the data from the UAV. Thus, the CDF of the RF link for the RR scheme is expressed as [33]

$$F_{\gamma_r^{\mathrm{RR}}}(\gamma) = \frac{1}{N_{\mathrm{M}}}\sum_{k=1}^{N_{\mathrm{M}}} F_{\gamma_k}(\gamma). \tag{15}$$

The ASB scheduling is to select the $\hat{k}$th MS, where $\hat{k} = \arg\max_k\{\gamma_k\}$, experiencing the largest instantaneous received SNR during a particular time slot. The CDF of the RF link for the ASB scheduling is obtained as [13]

$$F_{\gamma_r^{\mathrm{ASB}}}(\gamma) = \prod_{k=1}^{N_{\mathrm{M}}} F_{\gamma_k}(\gamma). \tag{16}$$

C. Outage Probability Analysis

This subsection presents the closed-form expression of the end-to-end outage probability. Moreover, we analyze the asymptotic outage probability in high transmit power regions and demonstrate how the nonlinear PAs and modulation schemes affect the outage probability.

1) Closed-Form Analysis: The overall CDF of SNDR for the UAV-aided FSO/RF DF relaying system is obtained as [34]

$$\begin{aligned} F_{\gamma_{\mathrm{end}}}(\gamma) &= \Pr[\min(\gamma_f, \gamma_r) \leq \gamma] \\ &= F_{\gamma_f}(\gamma) + F_{\gamma_r}(\gamma) - F_{\gamma_f}(\gamma)F_{\gamma_r}(\gamma), \end{aligned} \tag{17}$$

where $F_{\gamma_r}(\gamma)$ denotes the CDF of the SNDR γ_r of the RF link after multi-user scheduling schemes. Note that we can substitute $F_{\gamma_r}(\gamma)$ with (15) or (16) according to the multi-user scheduling. An outage of the system is encountered when the end-to-end SNDR γ falls below a predetermined threshold γ_{th}. By setting $\gamma = \gamma_{th}$ in (17), the outage probability can be rewritten as

$$p_{\mathrm{out}} = p_{\mathrm{out}}^{\mathrm{FSO}} + p_{\mathrm{out}}^{\mathrm{RF}} - p_{\mathrm{out}}^{\mathrm{FSO}} p_{\mathrm{out}}^{\mathrm{RF}}, \tag{18}$$

where $p_{\mathrm{out}}^{\mathrm{FSO}}$ and $p_{\mathrm{out}}^{\mathrm{RF}}$ are the outage probability of the FSO link and the RF link, respectively.

2) Asymptotic Analysis: For high FSO transmit power P_f, as the summation terms in (9) go to zero, we first express $p_{\mathrm{out}}^{\mathrm{FSO}}$ as

$$\lim_{P_f \to \infty} p_{\mathrm{out}}^{\mathrm{FSO}} = a_1. \tag{19}$$

Note that in high transmit regions, the outage probability of the FSO link is determined by link interruption due to the movement of the UAV [22]. Next, for the RF link, we consider high regimes of per-antenna transmit power P_a to show the fundamental impact on our system model with nonlinear PAs.

Proposition 2: For the case of high P_a, the outage probability of RF link under nonlinear PAs utilizing the EGT beamforming satisfies

$$\lim_{P_a \to \infty} p_{\mathrm{out},k}^{\mathrm{RF}} = \begin{cases} 0, & \gamma_{th} \leq \nu, \\ 1, & \gamma_{th} > \nu, \end{cases} \tag{20}$$

where ν is the SNDR ceiling defined as

$$\nu = \frac{S_{Q+1}^2}{S_{2Q} - S_{Q+1}^2}. \tag{21}$$

Proof: By taking the limit $P_a \to \infty$, we can calculate the dominant terms of $K - \gamma_{th}L$ in (13) with $i = j = Q$ as

$$K - \gamma_{th}L \approx |\alpha_Q|^2 P_a^Q \left(S_{Q+1}^2 - \gamma_{th}\left(S_{2Q} - S_{Q+1}^2\right)\right). \tag{22}$$

When $S_{Q+1}^2 - \gamma_{th}(S_{2Q} - S_{Q+1}^2) \geq 0$, $F_{\gamma_k}(\gamma_{th})$ in (13) goes to zero. With some basic algebra, we rewrite the condition in terms of γ_{th} as $\gamma_{th} \leq \frac{S_{Q+1}^2}{S_{2Q} - S_{Q+1}^2}$. Note that we can reveal $S_{2Q} - S_{Q+1}^2 \geq 0$ by Cauchy-Schwarz inequality. Otherwise, since $F_{\gamma_k}(\gamma_{th})$ goes to one when $S_{Q+1}^2 - \gamma_{th}(S_{2Q} - S_{Q+1}^2) < 0$, we can obtain the results of Proposition 2. □

Note that every MS has the same value ν since the SNDR ceiling ν is determined by the characteristics of the transmitter, such as modulation schemes and the non-linearity of PAs. Finally, substituting (19) and (20) into (18), regardless of multi-user scheduling schemes, we can obtain the end-to-end outage probability in high transmit power regions as

$$\lim_{P_f, P_a \to \infty} p_{\mathrm{out}} = \begin{cases} a_1, & \gamma_{\mathrm{th}} \leq \nu, \\ 1, & \gamma_{\mathrm{th}} > \nu. \end{cases} \tag{23}$$

For the linear PAs (i.e., $Q = 1$), the SNDR ceiling ν in (21) tends to infinity, implying no ceilings exist. However, for the nonlinear PAs (i.e., $Q \geq 3$), p_{out} goes to one for γ_{th} larger than ν. Since the ceiling can occur with any i.i.d. fading distributions in the high P_a regime, the performance under nonlinear PAs is limited by the SNDR ceiling. Moreover, we observe that modulation schemes affect ν in (21) since the constellation points of modulation schemes determine S_i. Thus, we will discuss how modulation schemes can affect the system with nonlinear PAs in the following subsection.

3) Special Cases for SNDR Ceilings: To better understand SNDR ceilings, we assume the data symbol s with particular modulations. First, we present the result of s with M-ary phase shift keying (PSK) modulations.

Corollary 1: M-ary PSK modulations are not affected by the SNDR ceilings.

Proof: For M-ary PSK modulations, $\mathbb{E}[|s|^i] = 1\ \forall i \in \mathbb{N}$. As $S_{2p} - S_{p+1}^2 = 0\ \forall p \in \mathbb{N}$, the SNDR ceilings for M-ary PSK is infinity. □

Note that as $L = 0$ in (11) regardless of P_a, utilizing M-ary PSK modulations can reduce the impact of nonlinear PAs.

TABLE II
SIMULATION PARAMETERS

	Symbol	Value	Symbol	Value
FSO link	ξ	$1.6\ \text{km}^{-1}$	A_0	5×10^{-3}
	w_{zeq}	2.0026 m	λ_f	1.55 um
	B_f	100 MHz	N_f	$10^{-14}\ \text{A}^2/\text{Hz}$
	θ_{FoV}	20 mrad	$C_n^2(0)$	$3 \times 10^{-13}\ \text{m}^{-\frac{2}{3}}$
	σ_{sp}	0.05 m	σ_{so}	0 mrad
	σ_{rp}	0.1 m	σ_{ro}	0.3 mrad
RF link	f	5 GHz	B_r	100 MHz
	N_0	-114 dBm /MHz	N_r	5
	$m_{\min}$	1	$m_{\max}$	4
UAV parameters	$E_{\max}$	639.36 kJ	T_{UAV}	500 s
	α_{up}	315	β_{up}	-211.261
	α_{hm}	308.709	β_{hm}	0.852
	α_{ho}	4.917	β_{ho}	275.204
	α_{dn}	68.956	β_{dn}	-65.183
	α_1	0.9018	α_2	0
	α_3	-0.4093 -0.1382ι	α_4	0
	α_5	0.0085 $+0.0035\iota$	α_6	0

TABLE III
COEFFICIENTS c_0 AND N_c FOR σ_R^2

σ_R^2	0-0.54	0.54-0.58	0.58-0.65	0.65-0.9	0.9-2	2-15
c_0	3.2	3.3	3.5	4	4.8	5.2
N_c	35	34	32	29	26	21

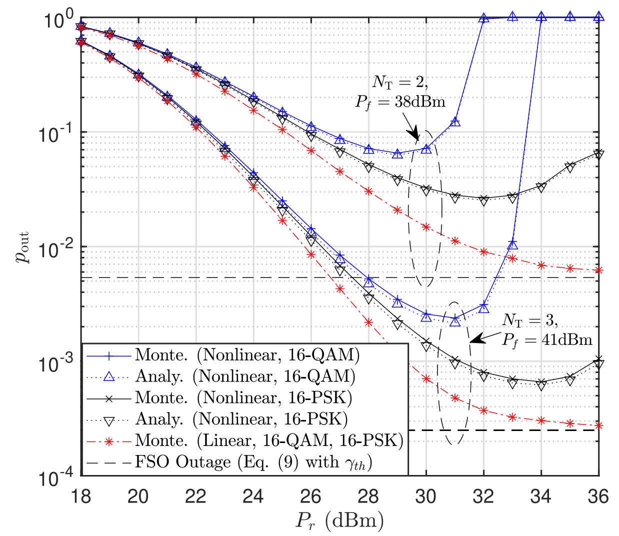

Fig. 2. Outage probabilities versus the transmit power P_r for $\mathbf{r}_u = (250, 250, 100)$m, and $\mathbf{r}_1 = (600, 600, 0)$m.

Next, we elaborate on the data symbol s following Gaussian distribution to attain fundamental insights into nonlinear PAs.

Lemma 1: When $s \sim \mathcal{CN}(0, 1)$, the SNDR ceiling is obtained as

$$\nu = \frac{\Gamma^2\left(\frac{Q+3}{2}\right)}{\Gamma\left(Q+1\right) - \Gamma^2\left(\frac{Q+3}{2}\right)}. \quad (24)$$

Proof: As $|s|$ follows Rayleigh distribution, the moments are given by $\mathbb{E}[|s|^i] = \Gamma(1 + \frac{i}{2})$. After some mathematical manipulations and simplifications with (21), we can obtain (24). □

Corollary 2: As the number of nonlinear components Q increases, the SNDR ceiling decreases when the data symbol s follows $\mathcal{CN}(0, 1)$. Moreover, the SNDR ceiling approaches zero when Q goes to infinity.

Proof: Please refer to Appendix B. □

When dealing with highly complex nonlinear systems that have Gaussian signals, it is only possible that the outage probability is less than one by reducing transmit power or increasing the number of antennas. However, other effective strategies for managing nonlinear systems, such as M-ary PSK, can significantly reduce the outage probability, avoiding the SNDR ceiling.

D. Numerical Results for Outage Probability

In this subsection, we present simulation results to verify the analytical and asymptotic expressions in Section III-C. We assume $r_s = (0, 0, 30)$m, $\omega = 1$, and $\gamma_{th} = 10$ dB. The other system parameters are listed in Table II and Table III. In Fig. 2, we compare the closed-form equation for the outage probability to Monte Carlo simulations to verify its accuracy when varying with modulation schemes, the number of antennas, and transmit power. We can observe that the analysis result in (18) matches the Monte-Carlo simulation results. However, a slight difference is due to the approximation used for a sum of Nakagami-m distribution. The outage probability of linear PAs converges to $p_{\text{out}}^{\text{FSO}}$ in (9) with γ_{th}, regardless of modulation schemes. When P_r is low, the performance of nonlinear PAs is similar to that of linear PAs. However, as the transmit power increases, the end-to-end outage probability of nonlinear PAs is non-monotonic against transmit power due to K and L in (12). Unlike linear PAs, modulation schemes affect the outage probability of nonlinear PAs. Specifically, 16-quadrature amplitude modulation (QAM) modulation is more affected by nonlinear PAs than 16-PSK modulation. Hence, the system with nonlinear PAs needs proper transmit power control and modulation schemes to prevent system outages.

Fig. 3 represents the end-to-end outage probability as a function of varying UAV and MS positions. We consider only one MS with the position as $r_1 = (x_1, 0, 0)$m and set the y-axis position of UAV to zero. The UAV's optimal position varies depending on the MS position. Specifically, when the position of x-axis for the MS is 500 m, the outage probability is minimized at the UAV position #1. Otherwise, when $x_1 = 700$ m and $x_1 = 900$ m, the UAV position #2 and #3 minimize the outage probability, respectively. Note that we can effectively minimize the outage probability by determining the optimal UAV position depending on the MS position.

In Fig. 4, we represent the end-to-end outage probability at different positions of the UAV for the multiuser scheduling

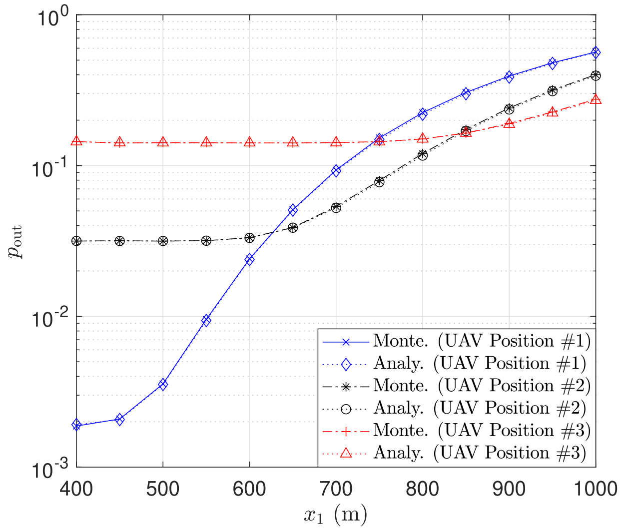

Fig. 3. Outage probability performance versus the x-axis position of the MS x_1 and the UAV position for $P_f = 38$ dBm, $P_r = 31.5$ dBm, $\theta_{\rm FoV} = 20$ mrad, $N_{\rm T} = 2$ and 16-QAM. The UAV position #1, #2, and #3 are $\mathrm{r}_u = (321, 0, 106)$ m, $\mathrm{r}_u = (427, 0, 83)$ m, and $\mathrm{r}_u = (576, 0, 51)$ m, respectively.

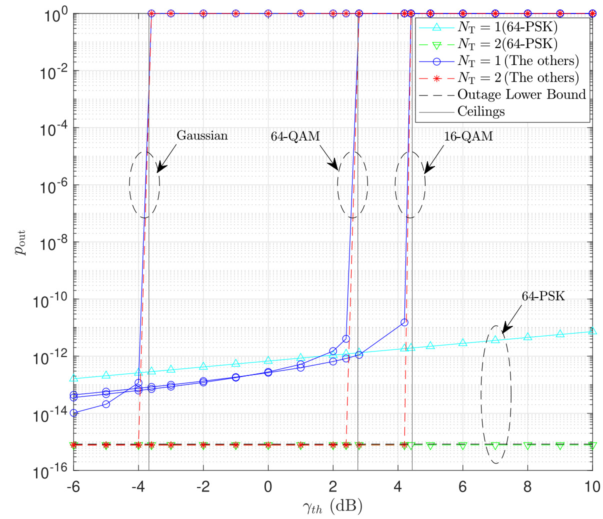

Fig. 5. Outage probability performance versus the SNDR thresholds for $P_f = 45$ dBm, $P_r = 61$ dBm, $\theta_{\rm FoV} = 25$ mrad, $\mathbf{r}_u = (100, 100, 100)$m, and $\mathbf{r}_1 = (2000, 2000, 0)$m.

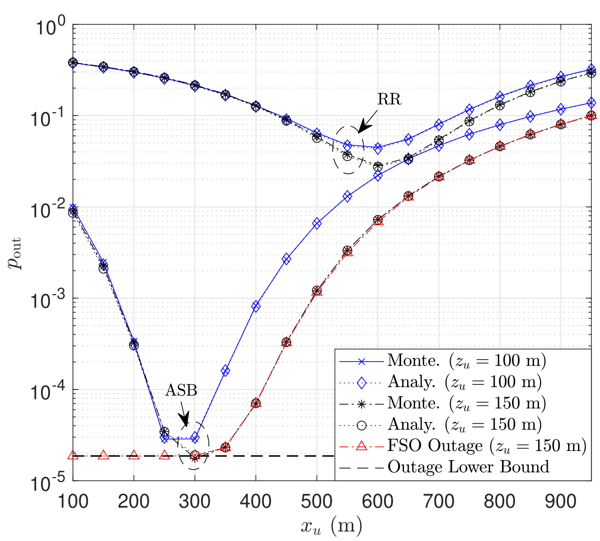

Fig. 4. Outage probability performance versus the x-axis position of the UAV x_u for $P_f = 41.5$ dBm, $P_r = 31.5$ dBm, $\theta_{\rm FoV} = 14$ mrad, $N_{\rm T} = 2$, $\mathbf{r}_1 = (350, 0, 0)$m, $\mathbf{r}_2 = (900, 0, 0)$m and 16-QAM.

schemes, such as the RR and the ASB cases. The ASB scheduling scheme performs better than the RR scheduling scheme since the ASB scheme utilizes the diversity of multiple MSs in RF links. In the ASB case at $\mathbf{r}_u = (300, 0, 150)$m, the end-to-end outage probability is minimized and asymptotically approaches outage lower bound a_1 in (23). Otherwise, the outage probability of the RR case is minimized when the UAV is located at $\mathbf{r}_u = (600, 0, 150)$m. Note that the optimal position of the UAV varies depending on the scheduling scheme, implying that determining the UAV position according to the scheduling scheme can significantly improve outage probability performance.

Fig. 5 shows the relationship between the outage probabilities and the SNDR ceilings in (23) with different modulations, i.e., Gaussian signaling, 16-QAM, 64-QAM, and 64-PSK as a function of the threshold γ_{th}. As expected, increasing the number of antennas decreases the outage probability for low γ_{th} regions. When $N_{\rm T} = 2$, the outage probability saturates to the outage lower bound a_1 in (23), implying that the dominant factor of end-to-end outage probability is the FSO links. For γ_{th} larger than υ, the outage rapidly converges to one except for 64-PSK, regardless of $N_{\rm T}$. The SNDR ceilings υ vary depending on the modulation schemes. As the number of constellation points increases, the SNDR ceiling decreases, making it difficult to use high-order modulations in high-threshold regions. However, as mentioned in Corollary 1, M-ary PSK modulations are unaffected by the ceiling. This means M-ary PSK modulations are more reliable than other modulations in high-threshold regions.

Figs. 2, 3, and 4 show that the derived closed-form of the outage probability matches the Monte-Carlo simulation. Moreover, optimizing transmit power and 3D placement according to scheduling schemes is necessary to minimize the outage probability of the UAV-aided FSO/RF system. To this end, we propose a joint optimization algorithm, which will be discussed in the following section.

IV. Joint 3D Placement and Transmit Power Optimization

In this section, we propose an iterative algorithm that jointly optimizes the 3D placement and transmit power in terms of minimizing the derived outage probability. Specifically, the algorithm can support both RR and ABS scheduling schemes by adjusting the parameters. We alternately optimize the transmit power P_r and 3D placement $\mathbf{r}_u$ by solving the problems while keeping the other variables fixed.

A. Problem Formulation

First, in order to optimize the UAV's 3D placement and transmit power, we formulate the end-to-end outage minimization problem as

$$\min_{\mathbf{r}_u, P_r} \quad p_{\text{out}} \tag{25a}$$

$$\text{s.t.} \quad E_{\text{UAV}} \leq E_{\max} \tag{25b}$$

$$P_r \leq P_{\text{lim}}, \tag{25c}$$

where E_{UAV} is the total energy consumption of the UAV,[1] $E_{\max}$ denotes the maximum available energy considering the battery capacity of the UAV, and P_{lim} is the transmit power constraint for the UAV. The problem (25) is hard to solve directly since (25) is a non-convex problem due to the non-convex objective function p_{out} and the non-convex constraint (25b). To tackle this issue, we solve the original problem (25) by partitioning the entire optimization variables into two blocks for the transmit power and the 3D placement.

B. Transmit Power Optimization

In this subsection, we convert (25) into the transmit power optimization problem for the fixed UAV's position. Then, as $p_{\text{out}}^{\text{FSO}}$ becomes constant, the transmit power optimization problem can be simplified as

$$\min_{P_r} \quad p_{\text{out}}^{\text{RF}} \tag{26a}$$

$$\text{s.t.} \quad P_r \leq P_{\max}, \ (25c), \tag{26b}$$

where $P_{\max}$ denotes the maximum available battery power and can be obtained by converting the constraint (25b) for P_r. To solve the non-convex problem (26), we utilize an analytical approach and employ the optimal power of a single MS case for both the RR and the ASB scheduling schemes.[2] As $\Gamma(a, x)$ is a monotonically decreasing function for $x \geq 0$, (26a) can be rewritten for kth MS as

$$\begin{aligned} \underset{P_r}{\text{argmin}}\, p_{\text{out},k}^{\text{RF}} &= \underset{P_r}{\text{argmax}}\ \Gamma\left(M_k, \frac{M_k \gamma_{th} \sigma_r^2}{\Omega_k g_k^2 (K - \gamma_{th} L)}\right) \\ &= \underset{P_r}{\text{argmax}} \sum_{i=1}^{Q} \sum_{j=1}^{Q} \alpha_i \alpha_j^* S_{i,j}^{SD} P_a^{\frac{i+j}{2}}, \end{aligned} \tag{27}$$

where $S_{i,j}^{SD} = S_{i,j}^{S} - \gamma_{th} S_{i,j}^{D}$. To solve (27), we define $q(P_a)$ as a derivative of (27) and find solutions $\hat{P}_a = \min\{P_a \in \mathbb{R}^+ | q(P_a) = 0\}$.[3] Note that $\hat{P}_a$ is only affected by nonlinear PAs and modulation schemes, regardless of the UAV's placement. Finally, with updating $P_{\max}$ at the given UAV's position, we efficiently determine the optimal transmit power considering the constraints (26b) as

$$P_r = \min\left\{N_{\text{T}} \hat{P}_a, P_{\max}, P_{\text{lim}}\right\}. \tag{28}$$

[1]For the detail definition of E_{UAV}, please refer to Appendix C.

[2]For detailed proof, please refer to Appendix D.

[3]For a detailed method for obtaining $\hat{P}_a$, please refer to Appendix E.

Algorithm 1: Proposed Algorithm for the Problem (25).

```
Initialize r_u ∈ C and calculate P̂_a.
while p_out has not converged do
    Determine P_r with (28) for given r_u.
    while r_u has not converged do
      Calculate ∇p_out with (30) for given P_r.
      Update r_u with (31).
    end while
    Calculate p_out(r_u, P_r) with (18).
end while
return r_u, P_r.
```

C. 3D Placement Optimization

Given the fixed transmit power P_r, we determine the 3D placement of the UAV while minimizing the outage probability. In this circumstance, the optimization problem of the UAV can be formulated as

$$\min_{\mathbf{r}_u} \quad p_{\text{out}}$$

$$\text{s.t.} \quad (25\text{b}). \tag{29a}$$

Since (29a) is non-convex with respect to $\mathbf{r}_u = \{x_u, y_u, z_u\}$, we alternatively adopt the gradient descent-based algorithm. The gradient of the outage probability ∇p_{out} with respect to $\mathbf{r}_u$ can be expressed as

$$\begin{aligned} \nabla p_{\text{out}} = &\ \nabla p_{\text{out}}^{\text{FSO}} + \nabla p_{\text{out}}^{\text{RF}} \\ &- p_{\text{out}}^{\text{RF}} \cdot \nabla p_{\text{out}}^{\text{FSO}} - p_{\text{out}}^{\text{FSO}} \cdot \nabla p_{\text{out}}^{\text{RF}}, \end{aligned} \tag{30}$$

where $\nabla p_{\text{out}}^{\text{FSO}}$ denotes the gradient of the FSO link.[4] In addition, $\nabla p_{\text{out}}^{\text{RF}}$ is the gradient of the RF links, which varies with multi-user scheduling schemes.[5] Considering constraint (25b), we update the position $\mathbf{r}_u$ using the gradient descent technique as follows

$$\mathbf{r}_u = P_{\mathcal{C}}\left(\mathbf{r}_u - \nabla p_{\text{out}}\right), \tag{31}$$

where $P_{\mathcal{C}}(x)$ is the projection operator defined as $P_{\mathcal{C}}(\mathbf{a}) = \text{argmin}_{\{x_a, y_a, v\} \in \mathcal{C}} ||z_a - v||$ and $\mathcal{C} = \{x, y, z \mid E_{\text{UAV}}(x, y, z) \leq E_{\max}\}$.[6] For satisfying constraint (25b), we fix the horizontal position and update only z_u since increasing z_u typically consumes more energy than moving horizontally.

The overall algorithm for optimizing the 3D placement and transmit power is summarized in Algorithm 1. The algorithm supports both the RR and the ASB scheduling schemes by substituting ∇p_{out} for the 3D placement. The proposed algorithm iteratively works until the outage probability is converged.

[4]Please refer to Appendix F for the derivations of $\nabla p_{\text{out}}^{\text{FSO}}$.

[5]The RF gradient of the outage probability with the RR and ASB schemes are expressed as $\nabla p_{\text{out}}^{\text{RF}} = \{d_x^{\text{RF}}, d_y^{\text{RF}}, d_z^{\text{RF}}\}$, with $d_j^{\text{RF}} = \frac{1}{N_{\text{M}}} \sum_{k=1}^{N_{\text{M}}} d_{k,j}^{\text{RF}}$ and $d_j^{\text{RF}} = \sum_{k=1}^{N_{\text{M}}} d_{k,j}^{\text{RF}} \prod_{i=1, i \neq k}^{N_{\text{M}}} p_{\text{out},i}^{\text{RF}}$ for $j \in \{x, y, z\}$, respectively. Please refer to Appendix G for the derivations of $d_{k,j}^{\text{RF}}$.

[6]To reduce the impact of the gradient vanishing problem, the gradient value (30) can be adjusted as $\nabla p_{\text{out}} = \frac{\epsilon_{pl} \nabla p_{\text{out}}}{||\nabla p_{\text{out}}||}$ if $||\nabla p_{\text{out}}|| < \epsilon_{pl}$.

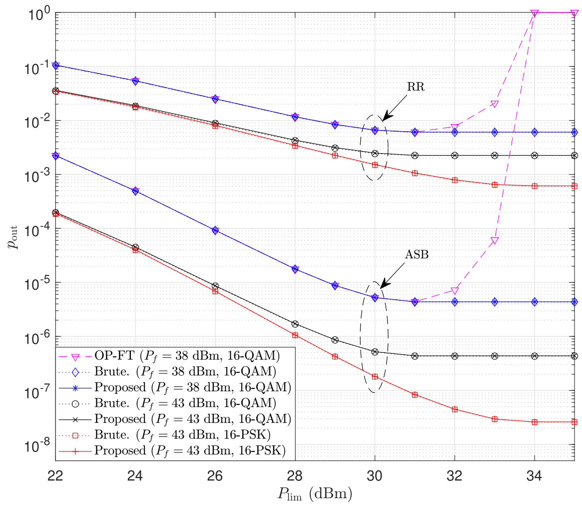

Fig. 6. Outage probability performance versus $P_{\rm lim}$ for $N_{\rm T} = 3$, $\mathbf{r}_1 = (800, 500, 0)$m and $\mathbf{r}_2 = (300, 500, 0)$m.

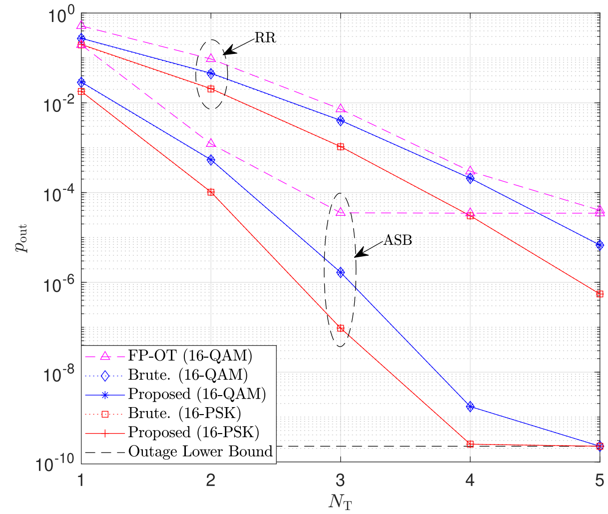

Fig. 7. Outage probability performance verse $N_{\rm T}$ for $P_f = 40$ dBm, $P_{\rm lim} = 36$ dBm, $\mathbf{r}_1 = (800, 500, 0)$m, and $\mathbf{r}_2 = (300, 500, 0)$m.

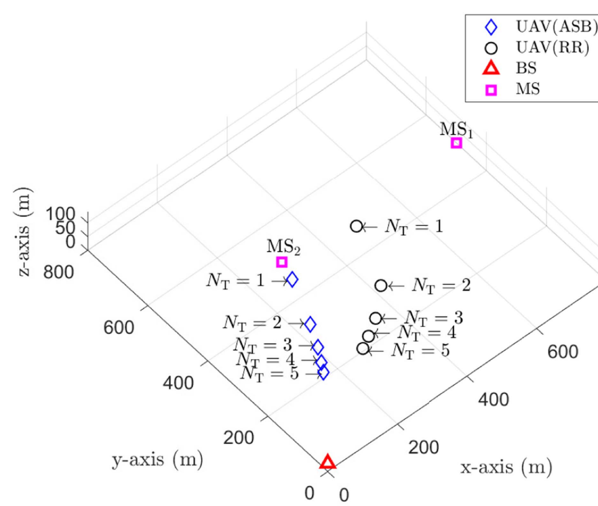

Fig. 8. Optimized 3D placement of the UAV varying with $N_{\rm T}$ when the RF links modulation is 16-QAM.

V. Simulation Results

In this section, we present simulation results to show the performance of the algorithm proposed in Section IV for the mixed FSO/RF UAV-aided relaying systems. We consider $\epsilon_{pl} = 10^{-2}$ and the other simulation parameters listed in Section III-D. For the comparison, we offer several comparable schemes.

- *Brute-force search with the EGT beamforming:* Brute-force search finds the minimum outage probability for every position over a 3D lattice with 1-m spacing, and every transmit power with 0.1-dBm spacing. It serves as an optimal baseline in this paper.
- *Optimized 3D placement with the RF constraint power (OP-FT):* OP-FT denotes the scheme optimizing the 3D placement with the Brute-force search while considering the RF constraint power as the transmit power, i.e., $P_r = P_{\rm lim}$.
- *Fixed 3D placement with the optimized transmit power (FP-OT):* FP-OT denotes the scheme optimizing the transmit power with the Brute-force search when UAV's position is fixed as $\mathbf{r}_u = (200, 200, 100)$m.

Fig. 6 illustrates the outage probability as a function of the transmit power constraint varying with modulation and multi-user scheduling schemes. We observe that the proposed algorithm performance is comparable to the Brute-force Search, regardless of the modulation type and multi-user scheduling schemes. The OP-FT degrades severely in high $P_{\rm lim}$ regions as power control is not adequately performed. With the proposed algorithm, when $P_{\rm lim}$ and P_f increase, the outage probability decreases. However, the outage probability remains constant when $P_{\rm lim}$ is larger than 31 dBm for 16-QAM and 34 dBm for 16-PSK since the transmit power is fixed to an optimal value according to the modulation scheme. As mentioned in Corollay 1, 16-PSK modulation performs better in high $P_{\rm lim}$ regions since 16-PSK modulation is less affected by nonlinearity.

In Fig. 7, we evaluate the outage probability verses $N_{\rm T}$. The results indicate that the proposed algorithm and the brute-force search technique have similar outage probabilities for all $N_{\rm T}$. In comparison with the RR scheduling schemes, the ASB scheme has a lower outage probability since the ASB scheme serves an MS with the best channel condition. Especially, the ASB scheme for 16-PSK reaches an outage lower bound a_1 of (23) when $N_{\rm T} = 5$. Moreover, the FP-OT shows a poor outage probability compared to the proposed algorithm, implying that optimizing the 3D placement of the UAV can further improve the outage probability.

Fig. 8 illustrates the optimized 3D placement of the UAV as a function of $N_{\rm T}$, when the proposed algorithm achieves the minimized outage probability as shown in Fig. 7. As increasing the number of antennas improves the performance of both the ASB and RR scenarios for the RF link, the UAV's position is closer to the BS in order to improve the FSO links. In the ABS case, the UAV is positioned close to the MS$_2$, which has better channel conditions on average. However, in the RR case,

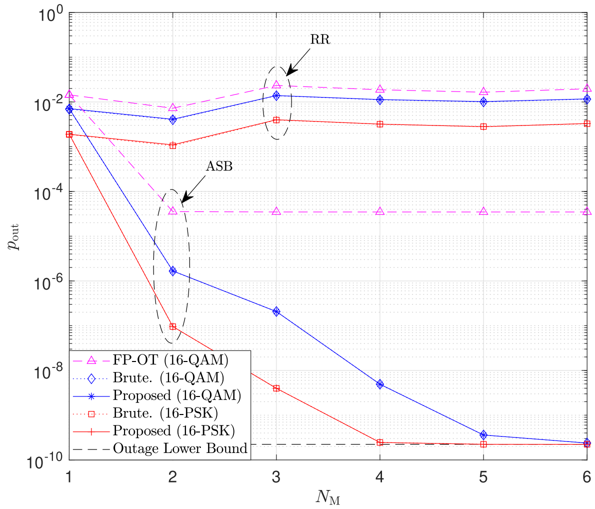

Fig. 9. Outage probability performance verse N_{M} for $N_{\text{T}} = 3, P_f =$ 40 dBm, and $P_{\text{lim}} = 36$ dBm.

TABLE IV
LOCATIONS OF MSs

k	x_k	y_k	z_k	k	x_k	y_k	z_k
1	800 m	500 m	0 m	4	600 m	600 m	0 m
2	300 m	500 m	0 m	5	300 m	800 m	0 m
3	800 m	800 m	0 m	6	800 m	700 m	0 m

the UAV is positioned equidistant from all MSs to provide fair support.

The outage probabilities are plotted as a function of the number of MSs in Fig. 9. The positions of MSs are given in Table IV. Regardless of N_{M}, the outage probability of the proposed algorithm similarly achieves that of the Brute-force search. Similar to Fig. 7, it is noted that the outage probability does not decrease in the FP-OT with both the RR and ASB cases, which results from the outage probability of the FSO link remaining constant. Moreover, regardless of N_{M} and modulation scheme, the outage probability is saturated in the RR case. However, as increasing N_{M}, the outage probability of the ASB scheme approaches the lower bound a_1. This is because the RR scheme allocates equal resources to all MSs, while the ASB scheme utilizes the diversity of multiple MSs.

The outage probability of the proposed algorithm is equivalent to the Brute-force Search for various simulation environments, implying that the algorithm effectively finds the optimal UAV's transmit power and 3D placement. Moreover, the proposed algorithm performs in the RR and ASB cases and can be applied to various multiuser schemes.

VI. CONCLUSION

This paper investigated the mixed FSO/RF relaying systems where the UAV serves as a DF relay with nonlinear PAs. Considering the channel characteristics of FSO and RF links, we analyzed closed-form and asymptotic expressions for the outage probabilities of the system where the multiple MSs are served with the RR and ASB scheduling schemes. Moreover, in MISO systems with EGT beamforming, we analyzed the effects of nonlinear PAs and demonstrated the existence of SNDR ceilings determined by modulation schemes. Based on the derived outage probability, we formulated the optimization problem and proposed the algorithm to find the UAV's 3D placement and transmit power. Specifically, we have designed an iterative algorithm that alternately solves the transmit power and the 3D placement. The proposed algorithm found the UAV's 3D placement and transmit power, which achieved the outage probability equivalent to the minimum outage probability. From the proposed algorithm, it is possible to enhance the system performance by fully utilizing the benefits of UAV-aided relaying systems.

APPENDIX A
COEFFICIENTS OF EQUATION (9)

In (9), the coefficients c_1, c_2, and c_3 are defined as $c_1 = c_3 c_0^{n+\beta_f-\tau} - c_2 c_0^{n+\alpha_f-\tau}$, $c_2 = c_4 c_6$, and $c_3 = c_4 c_5$, where

$$c_4 = \frac{\pi\tau}{\Gamma(\alpha_f)\Gamma(\beta_f)\sin(\pi(\alpha_f-\beta_f))}, \tag{32}$$

$$c_5 = \frac{(\alpha_f\beta_f)^{n+\beta_f}}{(n+\beta_f-\tau)\Gamma(n-\alpha_f+\beta_f+1)\,n!}, \tag{33}$$

and

$$c_6 = \frac{(\alpha_f\beta_f)^{n+\alpha_f}}{(n+\alpha_f-\tau)\Gamma(n+\alpha_f-\beta_f+1)\,n!}. \tag{34}$$

In addition, c_0 is the coefficient correlated with Rytov variance σ_R^2 [23].

APPENDIX B
PROOF OF COROLLARY 2

The SNDR ceiling in (24) can be rewrite as $\nu = \frac{1}{g(Q)-1}$, where $g(Q) = \frac{\Gamma(Q+1)}{\Gamma^2(\frac{Q+3}{2})}$. The first derivatives of $g(Q)$ is obtained as

$$g'(Q) = \frac{\Gamma(Q+1)}{\Gamma^2\left(\frac{Q+3}{2}\right)}\left(\psi^0(Q+1) - \psi^0\left(\frac{Q+3}{2}\right)\right), \tag{35}$$

where $\psi^0(x)$ denote the digamma function. Since $\psi^0(x)$ is strictly increasing on $(0,\infty)$, $\psi^0(Q+1) \geq \psi^0(\frac{Q+3}{2})$ for $Q \geq 1$. Thus, $g(Q)$ is an increasing function for $Q \geq 1$ (i.e., $g'(Q) \geq 0$). Moreover, we obtain that ν is a decreasing function of $g(Q)$ since $\nu'(g(Q)) < 0$. Therefore, as Q increases for $Q \geq 1$, $g(Q)$ increases and ν decreases. Moreover, when Q approaches infinity, $g(Q)$ tends to infinity and ν goes to zero.

APPENDIX C
THE DEFINITION OF E_{UAV}

E_{UAV} is the total energy consumed by the UAV, which is the sum of the energy required for data transmission and the energy consumed by the mechanical parts of the UAV during hovering, upward, downward, and horizontal movement. E_{UAV} is defined as

$$E_{\text{UAV}} = \underbrace{(\alpha_{\text{up}}(z_u - z_s) + \beta_{\text{up}})}_{E_{\text{Upward}}} + \underbrace{(\alpha_{\text{dn}}(z_u - z_s) + \beta_{\text{dn}})}_{E_{\text{Downward}}} + \underbrace{2\left(\alpha_{\text{hm}}\sqrt{(x_u - x_s)^2 + (y_u - y_s)^2} + \beta_{\text{hm}}\right)}_{E_{\text{Horizontality}}} + \underbrace{(\alpha_{\text{ho}}(z_u - z_s) + \beta_{\text{ho}})\,T_{\text{UAV}}}_{E_{\text{Hovering}}} + \underbrace{T_{\text{UAV}}P_r}_{E_{\text{Transmission}}} \tag{36}$$

where T_{UAV} is the time when UAV provides communication services. Moreover, $\alpha_{\text{up}}, \beta_{\text{up}}, \alpha_{\text{hm}}, \beta_{\text{hm}}, \alpha_{\text{ho}}, \beta_{\text{ho}}, \alpha_{\text{dn}}$, and β_{dn} are the constants related to the mechanical movement of the UAV [35]. The UAV flies from BS and provides communication services for T_{UAV} seconds after moving to a location that minimizes the outage probability. After providing the communication service for the predetermined time T_{UAV}, the UAV returns to the location of the BS.

Appendix D
The Optimal Power for the Multiuser Schemes

For the RR scheduling schemes, we can rewrite the objective function (26a) and introduce inequality as

$$\min_{P_r} \frac{1}{N_{\text{M}}}\sum_{k=1}^{N_{\text{M}}} p_{\text{out},k}^{\text{RF}} \geq \frac{1}{N_{\text{M}}}\sum_{k=1}^{N_{\text{M}}} \min_{P_r} p_{\text{out},k}^{\text{RF}}. \tag{37}$$

Since equality occurs in (37) when every MS has the same optimal transmit power, i.e., $\hat{P}_r = \text{argmin}_{P_r}\, p_{\text{out},k}^{\text{RF}}\ \forall k$, we utilize (28) as the optimal power for the RR case. For the ASB scheduling schemes, the objective function (26a) can be approximated with the incomplete gamma function as

$$\underset{P_r}{\text{argmin}} \prod_{k=1}^{N_{\text{M}}} p_{\text{out},k}^{\text{RF}} \approx \underset{P_r}{\text{argmin}} \prod_{k=1}^{N_{\text{M}}} \left(\frac{A_k}{K - \gamma_{th}L}\right)^{M_k}, \tag{38}$$

where $A_k = \frac{M_k \gamma_{th}\sigma_r^2}{\Omega_k g_k^2}$. Since A_k and M_k are positive values, the solution of (38) is the same as the optimal power for a single MS in (27).

Appendix E
The Detailed Method for Obtaining $\hat{P}_a$

The derivative of (27) is obtained as

$$q\left(P_a\right) = \sum_{i=1}^{Q}\sum_{j=1}^{Q}\left(\frac{i+j}{2}\right) P_a^{\frac{i+j}{2}-1}\alpha_i\alpha_j^* S_{i,j}^{SD}. \tag{39}$$

Since $q(P_a)$ is complicated by the polynomials with high degrees, we utilize 3rd-degree Taylor series expansion at $P_a = 0$ as

$$q\left(P_a\right) \approx q(0) + q'(0)P_a + \frac{1}{2}q''(0)P_a^2 + \frac{1}{6}q'''(0)P_a^3, \tag{40}$$

where

$$q(0) = |\alpha_1|^2 S_{1,1}^{SD}, \tag{41}$$

$$q'(0) = 4\cdot \text{Re}\left(\alpha_1\alpha_3^*\right) S_{1,3}^{SD}, \tag{42}$$

$$q''(0) = 12\cdot \text{Re}\left(\alpha_1\alpha_5^*\right) S_{1,5}^{SD} + 6|\alpha_3|^2 S_{3,3}^{SD}, \tag{43}$$

and

$$q'''(0) = 48\left(\text{Re}\left(\alpha_1\alpha_7^*\right) S_{1,7}^{SD} + \text{Re}\left(\alpha_3\alpha_5^*\right) S_{3,5}^{SD}\right). \tag{44}$$

The algebraic formula of the polynomial equation can find the solutions of $q(P_a) = 0$. Then, we take the real positive solution closest to zero as the solution $\hat{P}_a$.

Appendix F
The Derivation of $\nabla p_{\text{OUT}}^{\text{FSO}}$

The gradient of the FSO link is represented as $\nabla p_{\text{out}}^{\text{FSO}} = \{d_x^{\text{FSO}}, d_y^{\text{FSO}}, d_z^{\text{FSO}}\}$. To calculate d_x^{FSO} using the chain rule, we can express the gradient of the outage probability p_{out} with respect to x_u as follows

$$d_x^{\text{FSO}} = \frac{\partial p_{\text{out}}^{\text{FSO}}}{\partial\bar{\gamma}_f}\frac{\partial\bar{\gamma}_f}{\partial x_u} + \frac{\partial p_{\text{out}}^{\text{FSO}}}{\partial\alpha_f}\frac{\partial\alpha_f}{\partial\sigma_R}\frac{\partial\sigma_R}{\partial x_u} + \frac{\partial p_{\text{out}}^{\text{FSO}}}{\partial\beta_f}\frac{\partial\beta_f}{\partial\sigma_R}\frac{\partial\sigma_R}{\partial x_u}. \tag{45}$$

With some mathematical transformation, we can obtain $\frac{\partial\bar{\gamma}_f}{\partial x_u} = -\xi\bar{\gamma}_f D_f^{-1}(x_u - x_s)$ and $\frac{\partial\sigma_R}{\partial x_u} = \frac{11}{12}\sigma_R D_f^{-2}(x_u - x_s)$. Moreover, $\frac{\partial p_{\text{out}}^{\text{FSO}}}{\partial\bar{\gamma}_f}$, $\frac{\partial p_{\text{out}}^{\text{FSO}}}{\partial\alpha_f}$, $\frac{\partial\alpha_f}{\partial\sigma_R}$, $\frac{\partial p_{\text{out}}^{\text{FSO}}}{\partial\beta_f}$, and $\frac{\partial\beta_f}{\partial\sigma_R}$ are represented in (50) on the top of the next page, where $\text{csch}(\cdot)$ and $\cosh(\cdot)$ denote the hyperbolic cosecant function and the hyperbolic cosine function, respectively. Additionally, s_α, s_β, s_2 and s_3 in (50) are given as

$$s_\alpha = c_3 k_{3,\alpha} c_0^{n+\beta_f-\tau} - c_2 c_0^{n+\alpha_f-\tau}\left(k_{2,\alpha} + \log c_0\right) \tag{46}$$

$$s_\beta = c_3 c_0^{n+\beta_f-\tau}\left(k_{3,\beta} + \log c_0\right) - c_2 k_{2,\beta} c_0^{n+\alpha_f-\tau}, \tag{47}$$

$$s_2 = k_{2,\alpha} + \frac{1}{2}\log\frac{\gamma_{th}}{\bar{\gamma}_f} - \frac{1}{n+\alpha_f}, \tag{48}$$

and

$$s_3 = k_{3,\beta} + \frac{1}{2}\log\frac{\gamma_{th}}{\bar{\gamma}_f} - \frac{1}{n+\beta_f}, \tag{49}$$

respectively. The parameters $k_{i,\kappa}$ with $i \in \{2,3\}$ and $\kappa \in \{\alpha,\beta\}$ are given in (50). By similar approach to d_x^{FSO}, we can derive d_y^{FSO} with $\frac{\partial\bar{\gamma}_f}{\partial y_u} = -\xi\bar{\gamma}_f D_f^{-1}(y_u - y_s)$ and $\frac{\partial\sigma_R}{\partial y_u} = \frac{11}{12}\sigma_R D_f^{-2}(y_u - y_s)$. Moreover, d_z^{FSO} can be obtained with $\frac{\partial\bar{\gamma}_f}{\partial z_u} = -\xi\bar{\gamma}_f D_f^{-1}(z_u - z_s)$ and $\frac{\partial\sigma_R}{\partial z_u} = \sigma_R(\frac{11}{12}D_f^{-2}(z_u - z_s) - \frac{1}{200})$.

Appendix G
The Derivation of $d_{k,j}^{\text{RF}}$

Using the multi-variable chain rule, we reveal $d_{k,x}^{\text{RF}} = (\frac{\partial p_{\text{out},k}^{\text{RF}}}{\partial M_k}\frac{\partial M_k}{\partial m_k} + \frac{\partial p_{\text{out},k}^{\text{RF}}}{\partial\Omega_k}\frac{\partial\Omega_k}{\partial m_k})\frac{\partial m_k}{\partial\theta_k}\frac{\partial\theta_k}{\partial x_u} + \frac{\partial p_{\text{out},k}^{\text{RF}}}{\partial D_k}\frac{\partial D_k}{\partial x_u}$. After some mathematical transformation, we can obtain $d_{k,x}^{\text{RF}}$ as $d_{k,x}^{\text{RF}} = s_{d,k}(x_u - x_k)$, where

$$s_{d,k} = s_{o,k}\left(2 - \frac{s_{r,k}m_p|z_u - z_k|}{\sqrt{D_k^2 - (z_u - z_k)^2}}\right), \tag{51}$$

$$\frac{\partial p_{\text{out}}^{\text{FSO}}}{\partial \bar{\gamma}_f} = -\frac{(1-a_1)}{2}\sum_{n=0}^{N_c}\left(\frac{c_1}{\bar{\gamma}_f}\left(\frac{\gamma_{th}}{\bar{\gamma}_f}\right)^{\frac{\tau}{2}} + \frac{c_2}{\bar{\gamma}_f}\left(\frac{\gamma_{th}}{\bar{\gamma}_f}\right)^{\frac{n+\alpha_f}{2}} - \frac{c_3}{\bar{\gamma}_f}\left(\frac{\gamma_{th}}{\bar{\gamma}_f}\right)^{\frac{n+\beta_f}{2}}\right),$$

$$\frac{\partial p_{\text{out}}^{\text{FSO}}}{\partial \alpha_f} = (1-a_1)\sum_{n=0}^{N_c}\left(\frac{s_\alpha}{\tau}\left(\frac{\gamma_{th}}{\bar{\gamma}_f}\right)^{\frac{\tau}{2}} + \frac{c_2 s_2}{n+\alpha_f}\left(\frac{\gamma_{th}}{\bar{\gamma}_f}\right)^{\frac{n+\alpha_f}{2}} - \frac{c_3 k_{3,\alpha}}{n+\beta_f}\left(\frac{\gamma_{th}}{\bar{\gamma}_f}\right)^{\frac{n+\beta_f}{2}}\right),$$

$$\frac{\partial p_{\text{out}}^{\text{FSO}}}{\partial \beta_f} = (1-a_1)\sum_{n=0}^{N_c}\left(\frac{s_\beta}{\tau}\left(\frac{\gamma_{th}}{\bar{\gamma}_f}\right)^{\frac{\tau}{2}} + \frac{c_2 k_{2,\beta}}{n+\alpha_f}\left(\frac{\gamma_{th}}{\bar{\gamma}_f}\right)^{\frac{n+\alpha_f}{2}} - \frac{c_3 s_3}{n+\beta_f}\left(\frac{\gamma_{th}}{\bar{\gamma}_f}\right)^{\frac{n+\beta_f}{2}}\right),$$

$$\frac{\partial \alpha_f}{\partial \sigma_R} = \frac{0.49\sigma_R \operatorname{csch}^2\left(0.245\sigma_R^2\left(1+1.11\sigma_R^{\frac{12}{5}}\right)^{-\frac{7}{6}}\right)}{10\left(2.22\sigma_R^{\frac{12}{5}}-5\right)^{-1}\left(1+1.11\sigma_R^{\frac{12}{5}}\right)^{\frac{13}{6}}},\quad \frac{\partial \beta_f}{\partial \sigma_R} = \frac{0.51\sigma_R\left(1+0.69\sigma_R^{\frac{12}{5}}\right)^{-\frac{11}{6}}}{1-\cosh\left(0.51\sigma_R^2\left(1+0.69\sigma_R^{\frac{12}{5}}\right)^{-\frac{5}{6}}\right)},$$

$$k_{2,\alpha} = \frac{1}{c_2}\frac{\partial c_2}{\partial \alpha_f} = \log(\alpha_f\beta_f) + 1 + \frac{n}{\alpha_f} - \frac{1}{n+\alpha_f-\tau} - \pi - \psi^0(\alpha_f)\tan(\pi(\alpha_f-\beta_f)) - \psi^0(-\beta_f+n+\alpha_f+1),$$

$$k_{3,\alpha} = \frac{1}{c_3}\frac{\partial c_3}{\partial \alpha_f} = \frac{\beta_f+n}{\alpha_f} - \pi - \psi^0(\alpha_f)\tan(\pi(\alpha_f-\beta_f)) + \psi^0(\beta_f+n-\alpha_f+1),$$

$$k_{2,\beta} = \frac{1}{c_2}\frac{\partial c_2}{\partial \beta_f} = \frac{\alpha_f+n}{\beta_f} + \pi - \psi^0(\beta_f)\tan(\pi(\alpha_f-\beta_f)) + \psi^0(\alpha_f+n-\beta_f+1),$$

$$k_{3,\beta} = \frac{1}{c_3}\frac{\partial c_3}{\partial \beta_f} = \log(\alpha_f\beta_f) + 1 + \frac{n}{\beta_f} - \frac{1}{n+\beta_f-\tau} + \pi - \psi^0(\beta_f)\tan(\pi(\alpha_f-\beta_f)) - \psi^0(-\alpha_f+n+\beta_f+1). \quad (50)$$

with

$$s_{o,k} = \frac{1}{D_k^2\Gamma(M_k)}\left(\frac{\gamma_{th}}{\bar{\gamma}_k}\right)^{M_k}\exp\left(-\frac{\gamma_{th}}{\bar{\gamma}_k}\right), \quad (52)$$

and

$$s_{r,k} = \exp\left(\frac{\gamma_{th}}{\bar{\gamma}_k}\right)\left(\log\left(\frac{\gamma_{th}}{\bar{\gamma}_k}\right) - \psi^0(M_k+1) + 1\right) + \frac{2(\Omega_k - N_{\text{T}}\omega)}{m_k^{-1}\Omega_k}\left(\psi^0(m_k) - \psi^0\left(m_k+\frac{1}{2}\right) + \frac{1}{2m_k}\right). \quad (53)$$

Note that since calculating $\frac{\partial p_{\text{out},k}^{\text{RF}}}{\partial M_k}$ is complicated by the upper incomplete gamma function, we utilize $\frac{\partial p_{\text{out},k}^{\text{RF}}}{\partial M_k} \approx \frac{\partial p_{a,k}^{\text{RF}}}{\partial M_k}$, where

$$\frac{\partial p_{a,k}^{\text{RF}}}{\partial M_k} = \frac{1}{\Gamma(M_k+1)} \times \left(\log\left(\frac{\gamma_{th}}{\bar{\gamma}_k}\right) - \psi^0(M_k+1) + 1\right)\left(\frac{\gamma_{th}}{\bar{\gamma}_k}\right)^{M_k}$$

with $\bar{\gamma}_k = \frac{\Omega_k g_k^2(K-\gamma_{th}L)}{M_k\sigma_r^2}$. Similar to $d_{k,x}^{\text{RF}}$, we can calculate $d_{k,y}^{\text{RF}} = s_{d,k}(y_u - y_k)$ with the multi-variable chain rule after some mathematical manipulations and simplifications. Moreover, by similar approach to $d_{k,x}^{\text{RF}}$, we can calculate $d_{k,z}^{\text{RF}} = s_{z,k}(z_u - z_k)$ with

$$s_{z,k} = s_{o,k}\left(2 + \frac{s_{r,k}m_p\sqrt{D_k^2 - (z_u-z_k)^2}}{|z_u - z_k|}\right). \quad (54)$$

References

[1] Y. Zeng, R. Zhang, and T. J. Lim, "Wireless communications with unmanned aerial vehicles: Opportunities and challenges," *IEEE Commun. Mag.*, vol. 54, no. 5, pp. 36–42, May 2016.

[2] M. Mozaffari, W. Saad, M. Bennis, Y.-H. Nam, and M. Debbah, "A tutorial on UAVs for wireless networks: Applications, challenges, and open problems," *IEEE Commun. Surveys Tut.*, vol. 21, no. 3, pp. 2334–2360, thirdquarter 2019.

[3] W. Fawaz, C. Abou-Rjeily, and C. Assi, "UAV-aided cooperation for FSO communication systems," *IEEE Commun. Mag.*, vol. 56, no. 1, pp. 70–75, Jan. 2018.

[4] S. Zhang and N. Ansari, "3D drone base station placement and resource allocation with FSO-based backhaul in hotspots," *IEEE Trans. Veh. Technol.*, vol. 69, no. 3, pp. 3322–3329, Mar. 2020.

[5] S. Zhang and N. Ansari, "Latency aware 3D placement and user association in drone-assisted heterogeneous networks with FSO-based backhaul," *IEEE Trans. Veh. Technol.*, vol. 70, no. 11, pp. 11991–12000, Nov. 2021.

[6] D. Wu, X. Sun, and N. Ansari, "An FSO-based drone assisted mobile access network for emergency communications," *IEEE Trans. Netw. Sci. Eng.*, vol. 7, no. 3, pp. 1597–1606, Jul./Sep. 2020.

[7] X. Sun, N. Ansari, and R. Fierro, "Jointly optimized 3D drone mounted base station deployment and user association in drone assisted mobile access networks," *IEEE Trans. Veh. Technol.*, vol. 69, no. 2, pp. 2195–2203, Feb. 2020.

[8] L. Yu, X. Sun, S. Shao, Y. Chen, and R. Albelaihi, "Backhaul-aware drone base station placement and resource management for FSO-based drone-assisted mobile networks," *IEEE Trans. Netw. Sci. Eng.*, vol. 10, no. 3, pp. 1659–1668, May/Jun. 2023.

[9] J.-H. Lee, K.-H. Park, Y.-C. Ko, and M.-S. Alouini, "Throughput maximization of mixed FSO/RF UAV-aided mobile relaying with a buffer," *IEEE Trans. Wireless Commun.*, vol. 20, no. 1, pp. 683–694, Jan. 2021.

[10] G. Xu and Z. Song, "Performance analysis of a UAV-assisted RF/FSO relaying systems for internet of vehicles," *IEEE Internet Things J.*, vol. 9, no. 8, pp. 5730–5741, Apr. 2022.

[11] H. Ajam, M. Najafi, V. Jamali, and R. Schober, "Ergodic sum rate analysis of UAV-based relay networks with mixed RF-FSO channels," *IEEE Open J. Commun. Soc.*, vol. 1, pp. 164–178, 2020.

[12] L. Qu, G. Xu, Z. Zeng, N. Zhang, and Q. Zhang, "UAV-assisted RF/FSO relay system for space-air-ground integrated network: A performance analysis," *IEEE Trans. Wireless Commun.*, vol. 21, no. 8, pp. 6211–6225, Aug. 2022.

[13] P. K. Singya and M.-S. Alouini, "Performance of UAV-assisted multiuser terrestrial-satellite communication system over mixed FSO/RF channels," *IEEE Trans. Aerosp. Electron. Syst.*, vol. 58, no. 2, pp. 781–796, Apr. 2022.

[14] H. Kong, M. Lin, W.-P. Zhu, H. Amindavar, and M.-S. Alouini, "Multiuser scheduling for asymmetric FSO/RF links in satellite-UAV-terrestrial networks," *IEEE Wireless Commun. Lett.*, vol. 9, no. 8, pp. 1235–1239, Aug. 2020.

[15] H. Kong, M. Lin, J. Zhang, J. Ouyang, W.-P. Zhu, and M.-S. Alouini, "Beamforming design and performance analysis for satellite and UAV integrated networks in IoRT applications," *IEEE Internet Things J.*, vol. 9, no. 16, pp. 14965–14977, Aug. 2022.

[16] J. Jee, G. Kwon, and H. Park, "Precoding design and power control for SINR maximization of MISO system with nonlinear power amplifiers," *IEEE Trans. Veh. Technol.*, vol. 69, no. 11, pp. 14019–14024, Nov. 2020.

[17] Y. Zeng and R. Zhang, "Energy-efficient UAV communication with trajectory optimization," *IEEE Trans. Wireless Commun.*, vol. 16, no. 6, pp. 3747–3760, Jun. 2017.

[18] Y. Zeng, J. Xu, and R. Zhang, "Energy minimization for wireless communication with rotary-wing UAV," *IEEE Trans. Wireless Commun.*, vol. 18, no. 4, pp. 2329–2345, Apr. 2019.

[19] N. Babu, C. B. Papadias, and P. Popovski, "Energy-efficient 3-D deployment of aerial access points in a UAV communication system," *IEEE Commun. Lett.*, vol. 24, no. 12, pp. 2883–2887, Dec. 2020.

[20] Y. Chen, W. Feng, and G. Zheng, "Optimum placement of UAV as relays," *IEEE Commun. Lett.*, vol. 22, no. 2, pp. 248–251, Feb. 2018.

[21] M. T. Dabiri and S. M. S. Sadough, "Optimal placement of UAV-assisted free-space optical communication systems with DF relaying," *IEEE Commun. Lett.*, vol. 24, no. 1, pp. 155–158, Jan. 2020.

[22] J.-Y. Wang, Y. Ma, R.-R. Lu, J.-B. Wang, M. Lin, and J. Cheng, "Hovering UAV-based FSO communications: Channel modelling, performance analysis, and parameter optimization," *IEEE J. Sel. Areas Commun.*, vol. 39, no. 10, pp. 2946–2959, Oct. 2021.

[23] M. T. Dabiri, S. M. S. Sadough, and I. S. Ansari, "Tractable optical channel modeling between UAVs," *IEEE Trans. Veh. Technol.*, vol. 68, no. 12, pp. 11543–11550, Dec. 2019.

[24] E. Yanmaz, R. Kuschnig, and C. Bettstetter, "Achieving air-ground communications in 802.11 networks with three-dimensional aerial mobility," in *Proc. IEEE Int. Conf. Comput. Commun.*, Turin, Italy, 2013, pp. 120–124.

[25] Z. Ghassemlooy, W. Popoola, and S. Rajbhandari, *Optical Wireless Communications: System and Channel Modelling With MATLAB* . Boca Raton, FL, USA: CRC Press, 2019.

[26] G. Xu, N. Zhang, M. Xu, Z. Xu, Q. Zhang, and Z. Song, "Outage probability and average ber of UAV-assisted dual-hop FSO communication with amplify-and-forward relaying," *IEEE Trans. Veh. Technol.*, vol. 72, no. 7, pp. 8287–8302, Jul. 2023.

[27] Y. Zou et al., "Impact of power amplifier nonlinearities in multi-user massive MIMO downlink," in *Proc. IEEE Int. Conf. Comput. Commun. Workshops*, San Diego, CA, USA, 2015, pp. 1–7.

[28] J. J. Bussgang, "Crosscorrelation functions of amplitude-distorted Gaussian signals," Res. Lab. Electron., MIT, Cambridge, MA, USA, Tech. Rep. 216, 1952.

[29] N. N. Moghadam, G. Fodor, M. Bengtsson, and D. J. Love, "On the energy efficiency of MIMO hybrid beamforming for millimeter-Wave systems with nonlinear power amplifiers," *IEEE Trans. Wireless Commun.*, vol. 17, no. 11, pp. 7208–7221, Nov. 2018.

[30] M. Fozooni, M. Matthaiou, E. Bjornson, and T. Q. Duong, "Performance limits of MIMO systems with nonlinear power amplifiers," in *Proc. IEEE Glob. Commun. Conf.*, 2015, pp. 1–7.

[31] E. Bjornson, M. Matthaiou, and M. Debbah, "A new look at dual-hop relaying: Performance limits with hardware impairments," *IEEE Trans. Commun.*, vol. 61, no. 11, pp. 4512–4525, Nov. 2013.

[32] M. Simon and M.-S. Alouini, *Digital Communication Over Fading Channels*, 2nd ed.Hoboken, NJ, USA: Wiley, 2005.

[33] Y. Zou and G. Wang, "Intercept behavior analysis of industrial wireless sensor networks in the presence of eavesdropping attack," *IEEE Trans. Ind. Inform.*, vol. 12, no. 2, pp. 780–787, Apr. 2016.

[34] S. S. Ikki and S. Aissa, "A study of optimization problem for amplify-and-forward relaying over weibull fading channels with multiple antennas," *IEEE Commun. Lett.*, vol. 15, no. 11, pp. 1148–1151, Nov. 2011.

[35] H. V. Abeywickrama, B. A. Jayawickrama, Y. He, and E. Dutkiewicz, "Comprehensive energy consumption model for unmanned aerial vehicles, based on empirical studies of battery performance," *IEEE Access*, vol. 6, pp. 58383–58394, 2018.